

Noninteracting spherical active particles under confinement: generalized entropy potential

Yongfeng Zhao^{1,2,*}

¹*Center for Soft Condensed Matter Physics and Interdisciplinary Research & School of Physical Science and Technology, Soochow University, 215006 Suzhou, China*

²*School of Physics and Astronomy and Institute of Natural Sciences, Shanghai Jiao Tong University, Shanghai 200240, China*

(Dated: July 4, 2022)

We study the transport of self-propelled noninteracting active Brownian particles (ABPs) and run-and-tumble particles (RTPs) in a long tube with varying widths. We obtain a generalized Fick-Jacobs equation for the active particles under the condition of slow varying width and wide tubes. In the passive limit, it is equivalent to particles moving in a generalized entropy potential. The entropy potential resembles its counterpart for passive particles, with the activity changing the effective temperature and the effective width of the tube. The generalized entropy potential enables estimations of 1D steady-state density along the tube and the mean escape time out of a spindle chamber.

The transport of active particles along a long tube plays an essential role in many phenomena in biology and physics, especially if the shape of the tube is irregular and changes in width [1, 2]. For instance, asymmetric channels create a ratchet flow of active particles [3, 4]. As biological implications, during the infection of pathogens into a human body, microbes are transported along the tracheal, lymphangion, or blood vessels. The transport problem relates to special therapies, where engineered bacteria are transported along blood vessels to tumors, stimulating the immune system to kill cancer cells [5]. A natural system often endures hydrodynamics and complex interactions. However, as a starting point, knowledge of how simple active particles transport along a tube contributes to the studies of these processes. Specifically, we consider active Brownian particles (ABPs) and run-and-tumble particles (RTPs) [6, 7], which are often used in describing the motion of microbes such as bacteria [8–11].

Passive particles transported in channels have been studied for a long time [12–19]. In the seminal work of Jacobs [12], the time evolution of the 1D density of passive particles along a tube can be reduced to the Fick-Jacobs (FJ) equation, where the motion of the passive particles can be regarded as quasi-1D subject to an effective potential proportional to the local entropy. This concept simplifies the analysis of some phenomena, such as first-passage problems in tubes and stochastic resonance [20, 21].

It has not been fully explored, however, whether active particles moving in a long tube can be treated in the same framework. Unlike passive particles, active particles often accumulate around rigid walls [22–24] due to their persistent motion. Thus the 1D density of active particles is not proportional to the area of cross-sections of a tube, and a correction accounting for the boundary accumulation, which is proportional to the perimeter of the cross-sections, should be added. The correction will be significant if the persistence length of active particles is sufficiently large compared to the width of the tube.

Cases in the limit of narrow tubes and large translational

thermal noises have been discussed [4], where the width of the tube is comparable to the diameter of particles. The result extends the FJ framework and shows that a conservative potential cannot characterize the interaction between the activity of particles and the boundaries, and asymmetric channels can provoke ratchet flow along the tube. The channels of intermediate and large widths remain unexplored.

In this article, we analytically calculate the time evolution of the 1D probability density of active particles moving in long channels with rigid boundaries and show that the system can be reduced to 1D particles moving in an effective entropy potential in the passive limit. The activity of particles not only contributes to the effective temperature in the potential but also influences the effective width of the channel sensed by the particles. Then from the effective entropy potential, we show how to estimate the steady-state 1D density, the ratchet flow, and the mean-first-passage time of a particle escaping from a spindle channel.

I. THE FICK-JACOBS EQUATION OF PASSIVE PARTICLES

Consider passive Brownian particles with diffusion constant D moving in a long channel with hard nonslip boundaries along the x -axis, with sectional area $A(x)$ as a function of position x . The time evolution of the multidimensional probability density $P(\mathbf{r})$ satisfies the diffusion equation $\partial_t P = D \Delta P$, with nonslip boundary conditions $\mathbf{n} \cdot \nabla P = 0$, where \mathbf{n} is unit vectors normal to the boundaries.

If $A(x)$ is a slow-varying function of x , the time evolution of the 1D density profile $\rho(x) = \int P(\mathbf{r}) dS$ can be described by the Fick-Jacobs equation, which can be obtained by integrating the diffusion equation along all the spatial dimensions other than x [12, 13],

$$\partial_t \rho = D \partial_{xx} \rho + \partial_x [\rho(x) V'(x)], \quad (1)$$

with an 1D effective entropy potential $V(x) = -D \log A(x)$.

* yfzhao2021@suda.edu.cn

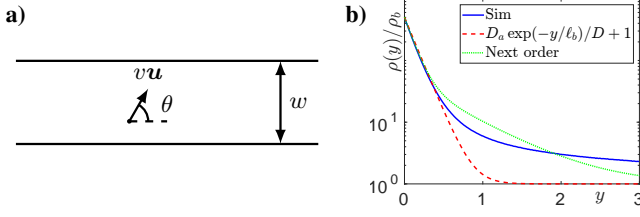


FIG. 1. **The steady-state density profile of active particles inside homogeneous tubes sketched in (a).** We impose periodic boundary condition in the x direction. The wall is located at $y = 0$. The green curves are obtained by preserving a finite \mathbf{Q} and assuming the third moment can be neglected. $\tau = 100$, $w = 10^4$, $v = 1$, $D = 0.1$.

II. ACTIVE PARTICLES UNDER CONFINEMENT WITH NONSLIP BOUNDARY CONDITIONS

We briefly revise the calculations of the steady-state density profile of ABPs in a channel with nonslip flat boundaries in Ref. [24]. (For AOUPs, refer to Ref. [25].) Some references assuming a vanishing thermal translational noise [26, 27] are beyond the scope of this article. Consider self-propelled particles with constant speed v and persistence time τ , subjected to thermal translational diffusion with constant D . The channel is translationally symmetric along the x -axis with width w . The boundaries are located at $y = 0$ and w (Fig. 1a).

Here we consider 2D noninteracting spherical ABPs for clarity. The calculations for RTPs are similar. The trajectory $\mathbf{r}(t)$ of a single particle can be described by the Itô-Langevin equations

$$\dot{\mathbf{r}} = v\mathbf{u}(\theta) + \sqrt{2D}\boldsymbol{\xi}(t), \quad \dot{\theta} = \sqrt{2/\tau}\eta(t). \quad (2)$$

$\boldsymbol{\xi}(t)$ and $\eta(t)$ are Gaussian white noises satisfying $\langle \xi_i(t)\xi_j(t') \rangle = \delta_{ij}\delta(t-t')$, $\langle \eta(t)\eta(t') \rangle = \delta(t-t')$. $\mathbf{u}(\theta) \equiv (\cos\theta, \sin\theta)$ is the orientation vector of the particle. The Fokker-Planck (FP) equation of the probability density function (PDF) $\Phi(\mathbf{r}, \mathbf{u}; t)$ of 2D ABPs is

$$\partial_t \Phi = -\nabla \cdot (v\mathbf{u}\Phi) + D\Delta\Phi + (1/\tau)\partial_{\theta\theta}\Phi. \quad (3)$$

Denoting $\rho(y) \equiv \langle \sum_i \delta(y - y_i) \rangle$ as the 1D density profile of the particles, $\mathbf{m}(y) \equiv \langle \sum_i \mathbf{u}_i \delta(y - y_i) \rangle$ as the orientation profile, and $\mathbf{Q}(y) \equiv \langle \sum_i (\mathbf{u}_i \mathbf{u}_i - \mathbf{I}/2) \delta(y - y_i) \rangle$ as the nematic tensor, we have the same dynamic equations valid for both ABPs and RTPs [6, 7] $\partial_t \rho = -v\nabla \cdot \mathbf{m} + D\Delta\rho$, $\partial_t \mathbf{m} = -(v/2)\nabla\rho - v\nabla \cdot \mathbf{Q} - \mathbf{m}/\tau + D\Delta\mathbf{m}$. The flow of particles with orientation \mathbf{u} is $\mathbf{\Gamma} \equiv v\mathbf{u}(\theta)\Phi(\mathbf{r}, \mathbf{u}; t) - D\nabla\Phi$, where $\Phi(\mathbf{r}, \mathbf{u}; t)$ is the probability density function of finding a particle at position \mathbf{r} with orientation \mathbf{u} . The nonslip boundary condition $\mathbf{e}_y \cdot \mathbf{\Gamma} = 0$ now reads $vm_y = D\rho'(y)$, $v(\rho/2 + Q_{yy}) = Dm'_y$ at $y = 0$ and w .

Consider the translational symmetry of the system along x , $m_x = 0$ and $Q_{yx} = 0$. To close the equations, we assume $\mathbf{Q} = \mathbf{0}$. If $w \gg \ell_b$, the density profile near $y = 0$ is

$$\rho_{\text{hm}}(y) \approx \rho_b(D_a e^{-y/\ell_b}/D + 1), \quad (4)$$

where $\ell_b \equiv D/\sqrt{(D_a + D)/\tau}$ is the characteristic length scale of the thickness of the boundary layer, $D_a \equiv v^2\tau/2$ is the active contribution of the effective diffusion constant, $D_{\text{eff}} \equiv D_a + D$, and ρ_b is the bulk density at $y = w/2$. Then $m_{\text{hm}}(y) \equiv m_y(y) = D\rho'(y)/v$. The result has been obtained in Ref. [22, 24]. The number of excess particles accumulated near the boundary can be estimated by $n_{\text{db}}\rho_b \equiv \rho_b \int_0^\infty dy D_a e^{-y/\ell_b}/D = \rho_b D_a \ell_b/D$.

Hence, truncating at the second order in the moment expansion of Φ , the $\rho_{\text{hm}}(y)$ near a hard boundary exponentially decreases away from the wall with a characteristic thickness ℓ_b . We test the approximation in quasi-1D agent-based simulations, where we reject the motion of a particle if it moves out of the confined region. The numerical results show a slower decay than Eq. (4), which is due to a nonzero $\nabla \cdot \mathbf{Q}$. A finer estimation can be obtained by truncating at a higher-order in the moment expansion of Φ , where we can identify more exponential components accounting for a slower decay. For $w \gg \ell_b$, ℓ_p , where the persistent length of the particle $\ell_p \equiv v\tau$, the approximation Eq. (4) provides reasonable estimation of $\rho_{\text{hm}}(y)$ (Fig. 1b).

III. FICK-JACOBS EQUATIONS OF ACTIVE PARTICLES IN 2D CHANNELS

Consider noninteracting ABPs/RTPs in a long channel in 2D with varying widths. The top and bottom boundaries of the channel are described by $y = w_1(x)$ and $y = w_2(x)$ respectively (Fig. 2a). Denoting $\tilde{\Phi}(x, \mathbf{u}) = \int_{w_1(x)}^{w_2(x)} \Phi(x, y, \mathbf{u}) dy$, if $|w'_i(x)| \ll 1$ the time evolution of $\tilde{\Phi}(x, \mathbf{u})$ reads

$$\partial_t \tilde{\Phi} = -v \cos\theta \partial_x \tilde{\Phi} + (1/\tau) \partial_{\theta\theta} \tilde{\Phi} + D \partial_x [\partial_x \tilde{\Phi} - \Phi^{\text{bd}} w'(x)], \quad (5)$$

where a zeroth order approximation is considered: $\Phi(x, w_{1,2}(x), \mathbf{u}) \approx \Phi^{\text{bd}}$, and Φ^{bd} is the boundary value of Φ calculated in a homogeneous channel. $w(x) \equiv w_2(x) - w_1(x)$.

Eq. (5) resembles the FJ equation if the boundary value Φ^{bd} can be related to $\tilde{\Phi}$, but an analytic solution of the FP equation in a homogeneous channel with nonslip boundary conditions is out of reach. We instead calculate the dynamics of the 1D integrated density $\tilde{\rho} \equiv \int \rho dy$ and the first moment $\tilde{m}_1 \equiv \int m_x dy$,

$$\partial_t \tilde{\rho} = -v \partial_x \tilde{m}_1 + D \partial_{xx} \tilde{\rho} - D \partial_x [\rho^{\text{bd}} w'(x)], \quad (6)$$

$$\partial_t \tilde{m}_1 = -\frac{v}{2} \partial_x (\tilde{\rho} + \tilde{m}_2) - \frac{\tilde{m}_1}{\tau} + D \partial_x [\partial_x \tilde{m}_1 - m_1^{\text{bd}} w'(x)], \quad (7)$$

where the second moment $\tilde{m}_2 \equiv 2 \int Q_{xx} dy$. The key assumption toward an FJ equation is $L \gg w(x)$ such that the local steady-state is reached in the y -direction at any x . Keeping only the terms of order $w'(x)$, near the boundaries the shifted density $\rho(x, |y - w_{1,2}(x)|)$ can be approximated by Eq. (4) with $w = w(x)$. Integration on y gives the relation between $\tilde{\rho}$ and ρ^{bd} , $\rho^{\text{bd}} = D_{\text{eff}} \tilde{\rho}/(Dw(x) + 2D_a \ell_b)$. The

density field is equivalent to being subjected to an effective potential

$$V(x) = -D_{\text{eff}} \log[2D_a \ell_b / D + w(x)] . \quad (8)$$

Unfortunately, the relation between m_1^{bd} and \tilde{m}_1 does not lead to the same potential Eq. (8) in the zeroth-order approximation because $m_1 = 0$ in homogeneous channels. Thus, in this regime, the activity of the particles only modifies the effective diffusion constant $D_{\text{eff}} \equiv D + v^2 \tau / 2$, and the effective potential Eq. (8), while the dynamics of the 1D density are passive if we consider \tilde{m}_1 to relax much faster than $\tilde{\rho}$ and if $\tilde{\rho}$ is smooth such that the higher-order derivatives can be neglected, $\partial_t \tilde{\rho} = D_{\text{eff}} \partial_{xx} \tilde{\rho} + \partial_x [\tilde{\rho} V'(x)]$. The effective potential Eq. (8), however, is not obtained by replacing the diffusion constant D in the passive entropy potential $V = -D \log w$ by D_{eff} , due to the accumulation of particles near boundaries. The boundary layer smooths the varying width of the channel by adding a constant $2n_{\text{bd}} = 2D_a \ell_b / D$ proportional to the number of excess particles accumulated near the two boundaries. Note $\ell_b \sim D_a^{-1/2}$ at sufficiently large D_a , and $n_{\text{bd}} \sim D_a^{1/2}$. At large D_a , a thin boundary layer can contribute significantly to the total density. The particles then spend most of the time near the boundary and do not sense the change in the width of the channel.

The \tilde{m}_1 field can be recovered by accounting for the slope of the boundaries. In the limit of wide channels $w \gg \ell_b$, we can assume local translational symmetry along the tangential direction of the boundaries. Then at the boundary, \mathbf{m} is locally normal to the boundary, and m_1^{bd} is \mathbf{m} projected on the x -axis. $m_1^{\text{bd}} = m_{\text{hm}}(0) \sin \arctan[w'(x)/2] \approx m_{\text{hm}}(0)w'(x)/2$. In the bulk $\mathbf{m} = 0$ and only the two nonzero boundary layers contribute to \tilde{m}_1 . $\tilde{m}_1 = 2 \int_0^\infty dy m_{\text{hm}}(y)w'(x)/2$. From Eq. (4), $m_1^{\text{bd}} = \tilde{m}_1 / 2\ell_b$. Thus the orientation field is equivalent to being subjected to another effective potential

$$V_m(x) = -D/(2\ell_b) \log w(x) . \quad (9)$$

Then we have the FJ-like equations for ABPs under the first order approximation of $w'(x)$,

$$\begin{aligned} \frac{\partial \tilde{\rho}}{\partial t} &= -v \frac{\partial \tilde{m}_1}{\partial x} + D \frac{\partial^2 \tilde{\rho}}{\partial x^2} + \frac{\partial}{\partial x} [\tilde{\rho} V'(x)] , \\ \frac{\partial \tilde{m}_1}{\partial t} &= -\frac{v}{2} \frac{\partial (\tilde{\rho} + \tilde{m}_2)}{\partial x} - \frac{\tilde{m}_1}{\tau} + D \frac{\partial^2 \tilde{m}_1}{\partial x^2} + \frac{\partial}{\partial x} [\tilde{m}_1 V'_m(x)] . \end{aligned} \quad (10)$$

$$(11)$$

The activity of the particles is partially restored. However, since $V_m(x) \neq V(x)$, a single conservative potential cannot describe the 1D dynamics of 2D ABPs.

IV. 1D STEADY-STATE DENSITY PROFILE AND RATCHET FLOW OF ABPS ALONG 2D CORRUGATED CHANNELS

Considering the zeroth-order approximation at large spatial-temporal scales, the 1D steady-state distributions of active particles in slow-varying channels have the form

of Boltzmann weights with the effective temperature D_{eff} , $\tilde{\rho}_{\text{ss}}(x) \propto \exp(-V(x)/D_{\text{eff}}) = 2n_{\text{bd}} + w(x)$. The calculations can be verified by agent-based simulations with both symmetric channels (Fig. 2b) and asymmetric channels (Fig. 2c-d). The results show that the 1D density profile flattened due to the existence of boundary layers. Because the number of particles absorbed by boundaries is independent of the width of the channel, its contribution to the density profile smooths out the effective potential and the density profile. We note that the approximation does not hold if $|w'(x)|$ is not small.

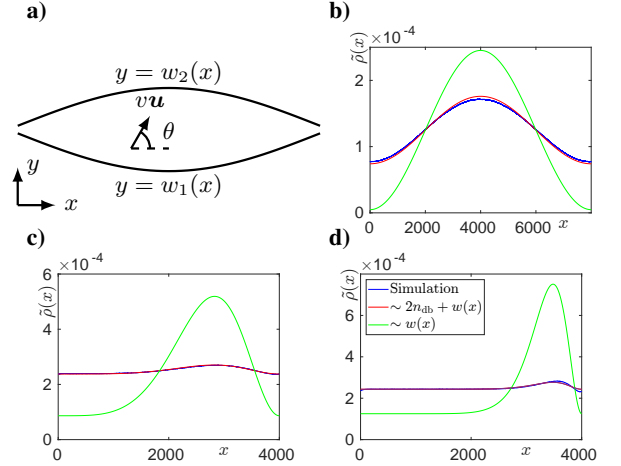


FIG. 2. **The 1D density profile of ABPs along a corrugated 2D channel sketched in (a).** The boundary is located at $y = w_{1,2}(x) = \pm[A(1 - \cos(2\pi x/L))/2 + C_0]$ with $A = 500$ (b), or $y = w_{1,2} = \pm[A(1 - \cos(2\pi(x/L)^N))/2 + C_0]$ with $N = 2$ (c) and $N = 5$ (d), $A = 50$. The theoretical estimation of the density profile is obtained by $\exp(-V(x)/D_{\text{eff}})$. The red lines are calculated using the $V(x)$ in Eq. (8), while the green lines are using the passive counterpart $V(x) = -D_{\text{eff}} \log w(x)$. $L = 8 \times 10^3$ (b) and 4×10^3 (c-d), $C_0 = 10$, $v = 5$, $\tau = 100$, $D = 0.1$.

Furthermore, asymmetric channels should provoke non-equilibrium ratchet flows, which cannot be estimated by equilibrium Boltzmann weights. The deviation of steady-state 1D density profile from the Boltzmann weights leads to the steady flow in asymmetric channels. The first-order approximation Eq. (10)-(11) assuming $\tilde{m}_2 = 0$ cannot fully account for the ratchet flow. But given the steady-state density profile measured from simulations, $V(x)$ predicts a weak ratchet flow by $J_{\text{tot}} \equiv \int J_x d^2 \mathbf{r} = - \int \tilde{\rho}_{\text{ss}}(x) V'(x) dx$, where $J_x = \langle \sum_i \dot{x}_i \delta(\mathbf{r} - \mathbf{r}_i) \rangle$ is the x -component of the flow field (Fig. 3).

V. GENERALIZATION TO 3D TUBES

The construct of the effective potential applies to 3D tubes along the x direction without loss of generality. However, we note that a large curvature of the boundary in the yz plane can also induce particle accumulations, and the full solution can thus be highly nontrivial [28]. Suppose the radius of the

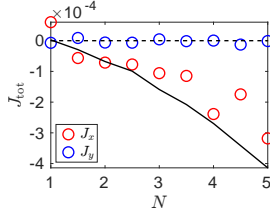


FIG. 3. **The ratchet flow of ABPs in asymmetric 2D channels.** The boundary is located at $y = w_{1,2} = \pm[A(1 - \cos(2\pi(x/L)^N))/2 + C_0]$ with varying N . The solid black curve shows the estimation of the total flow obtained by $-\int \rho_{ss}(x)V'(x)dx$, where $\rho_{ss}(x)$ is measured from the simulations. The dashed black curve shows $J = 0$. $A = 50$, $C_0 = 10$, $v = 5$, $\tau = 100$, $D = 0.1$.

boundaries of cross-sections is much larger than ℓ_p such that the density profile near a homogeneous flat boundary can approximate the density near the boundary. Then, the integration of the density profile in a cross-section in the yz plane can be estimated as the sum of contributions from bulk and boundary. We have $\tilde{\rho}(x) \approx \rho_b[A(x) + n_{db}P(x)]$, where $A(x)$ is the area of the cross-section of the tube along the yz plane at x , and $P(x)$ is the perimeter of the cross-section. Thus we have

$$V(x) = -D_{\text{eff}} \log [n_{db}P(x) + A(x)]. \quad (12)$$

Note that $n_{db} = D_a \ell_b / D$, where $D_a = v^2 \tau / d$ in d -dimensional space.

The steady-state 1D density can be estimated from Eq. (12) and tested with simulations of RTPs in a 3D tube with rotational symmetry along the x axis (Fig. 4b). Note that the estimation is valid only for sufficiently large C_0 to ensure that the curvature of the tube is neglectable. Otherwise, the accumulation of particles around a large curvature will further flatten the density profile (Fig. 4a). The agreement also indicates that the estimation from ABPs directly applies to RTPs because they share the same dynamics of ρ and \mathbf{m} .

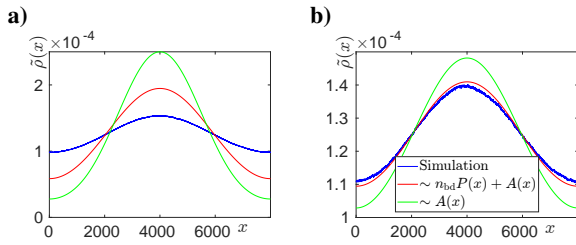


FIG. 4. **The 1D density profile of RTPs along a corrugated 3D tube.** The cross sections in yz plane is circular of radius $R(x) = R_0[1 - \cos(2\pi x/L)]/2 + C_0$. $C_0 = 50$ (a) and 500 (b). The theoretical estimation of the density profile is obtained by $\exp(-V(x)/D_{\text{eff}})$. The red lines are calculated using the $V(x)$ in Eq. (12), while the green lines are using the passive counterpart $V(x) = -2D_{\text{eff}} \log R(x)$. $L = 8 \times 10^3$, $R_0 = 100$, $v = 5$, $\tau = 100$, $D = 0.1$.

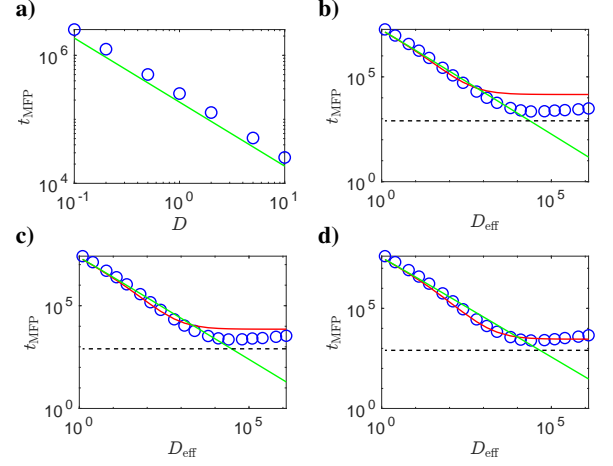


FIG. 5. **The mean first passage time of a passive particle (a) or an ABP (b-d) moving from the middle of a spindle ($x = L/2$) to one of the necks ($x = 0$ or L).** The width of the spindle is defined as $w(x) = A[1 - \cos(2\pi x/L)] + 2C_0$. $L = 8000$, $C_0 = 10$, $A = 100$ (b), 200 (c), and 500 (d). The simulation data are shown by the circles. The red lines are estimated from the effective potential given by Eq. (8), while the green lines are from $V(x) = -D \log A(x)$. The black dashed lines indicate the running time $L/(2v)$ for a particle from $x = L/2$ to one of the necks. $v = 5$ and $D = 0.1$ for the ABPs, and τ ranges from 10^{-1} to 10^5 .

VI. MEAN-ESCAPE TIME OF AN ACTIVE PARTICLE FROM A SPINDLE CHAMBER

With the generalized entropy potential (8), one can calculate the mean-first-passage time of one particle escaping from a spindle chamber (Fig. 1a). If $|V_m''(x)| \ll 1$, the mean-first-passage time t_{MFP} of a particle starting from the middle of the spindle $x = L/2$ with random orientation and reaching one of the necks at $x = 0$ or L is given by Kramer's seminal work [29, 30]

$$t_{\text{MFP}} \sim \frac{\pi}{2\sqrt{|V''(L/2)V''(0)|}} \exp \frac{V(0) - V(L/2)}{D_{\text{eff}}}. \quad (13)$$

For passive particles, $V = -D \log w(x)$, $t_{\text{MFP}} \propto 1/D$.

The $1/D$ scaling of passive particles can be checked from simulations (Fig. 5a). t_{MFP} for active particles, however, does not follow the $1/D_{\text{eff}}$ scaling because the activity contributes to both the effective diffusion constant and the effective width of the channel. The MFPT first decreases with D_{eff} , similar to passive particles, and then starts to increase at an optimal D_{eff} (Fig. 5b). Unlike passive particles, ABPs have finite moving speed, and the time for ABPs to travel $L/2$ is bounded by $L/(2v)$. For larger D_{eff} , the time for ABPs to stay near the boundary increases with τ . Thus the time for ABPs to escape from the channel increases. Note that Eq. (13) with the effective potential Eq. (8) qualitatively describe the transition away from the passive regime. At large τ the condition that $w \gg \ell_p$ cannot be held and Eq. (8) fails. Thus, quantitative agreement at large D_{eff} cannot be expected.

VII. DISCUSSION

In this article, we extended the Fick-Jacobs equation from passive particles to active particles in the limit of a wide tube $w(x) \gg \ell_b$ with slow varying width $|w'(x)| \ll 1$ when the boundary layers and the bulk can be separated. We show that the generalized entropy potential can better predict the steady-state 1D density profile along the tube than simply replacing the diffusion constant with its effective counterpart and qualitatively give the mean-first-passage time from Kramers' law. We use ABPs in the analysis, but all the calculations hold automatically for RTPs because ABPs and RTPs share the same dynamics of the density field and the orientation field [6, 7], which is used in the analysis. Note that the calculations require a finite D , which leads to a continuous density profile near the boundary and nonzero ℓ_b .

How to account for the deviation from the local steady state in the y -direction at finite $w'(x)$ remains a challenging question. Another limitation of the work is that we assume the nematic tensor \mathbf{Q} to be vanishing, which requires $w(x) \gg \ell_p$. The higher-order moments important for the density profile remain out of reach.

In this work, dilute spherical particles are considered. Elongated active particles can align with rigid boundaries and ac-

cumulate as well [31]. The probability of particles leaving boundaries decreases with a larger aspect ratio, and the number of accumulated particles increases with the length of the particle in the dilute limit [31]. A more significant boundary effect can be expected with elongated particles. For dense particles, the interactions reshape the density profiles near the wall. Particles with repulsive interactions have boundary layers with larger widths and smaller densities because of volume exclusion [32].

A possible relevant experimental setup can be colloid particles driven by an external magnetic field moving in PDMS microfluid channels if the contribution from hydrodynamics of the water can be neglected and the boundaries can be considered rigid walls. Robots moving on a track with varying widths could be a cleaner experimental system.

ACKNOWLEDGMENTS

The author thanks Xiaqing Shi, Hepeng Zhang, Hugues Chaté, and Masaki Sano for helpful discussions and critical comments. The author acknowledges support from the start-up grant from Soochow University.

-
- [1] J. chun Wu, Q. Chen, and B. quan Ai, Entropic transport of active particles driven by a transverse ac force, *Physics Letters A* **379**, 3025 (2015).
 - [2] L. Caprini, F. Cecconi, and U. Marini Bettolo Marconi, Transport of active particles in an open-wedge channel, *The Journal of Chemical Physics* **150**, 144903 (2019), <https://doi.org/10.1063/1.5090104>.
 - [3] B.-Q. Ai, Y.-F. He, and W.-R. Zhong, Entropic ratchet transport of interacting active brownian particles, *The Journal of Chemical Physics* **141**, 194111 (2014), <https://doi.org/10.1063/1.4901896>.
 - [4] P. Maggaretti and H. Stark, Model microswimmers in channels with varying cross section, *The Journal of Chemical Physics* **146**, 174901 (2017), <https://doi.org/10.1063/1.4981886>.
 - [5] L. Shi, B. Yu, C.-H. Cai, W. Huang, B.-J. Zheng, D. K. Smith, and J.-D. Huang, Combined prokaryotic-eukaryotic delivery and expression of therapeutic factors through a primed autocatalytic positive-feedback loop, *Journal of Controlled Release* **222**, 130 (2016).
 - [6] M. E. Cates and J. Tailleur, When are active Brownian particles and run-and-tumble particles equivalent? Consequences for motility-induced phase separation, *Europhys. Lett.* **101**, 20010 (2013).
 - [7] A. P. Solon, M. E. Cates, and J. Tailleur, Active brownian particles and run-and-tumble particles: A comparative study, *The European Physical Journal Special Topics* **224**, 1231 (2015).
 - [8] H. C. Berg and D. A. Brown, Chemotaxis in *Escherichia coli* analysed by three-dimensional tracking, *Nature* **239**, 500 (1972).
 - [9] L. G. Wilson, V. A. Martinez, J. Schwarz-Linek, J. Tailleur, G. Bryant, P. N. Pusey, and W. C. K. Poon, Differential dynamic microscopy of bacterial motility, *Phys. Rev. Lett.* **106**, 018101 (2011).
 - [10] V. A. Martinez, R. Besseling, O. A. Croze, J. Tailleur, M. Reufer, J. Schwarz-Linek, L. G. Wilson, M. A. Bees, and W. C. K. Poon, Differential dynamic microscopy: A high-throughput method for characterizing the motility of microorganisms, *Biophys. J.* **103**, 1637 (2012).
 - [11] A. Curatolo, N. Zhou, Y. Zhao, C. Liu, A. Daerr, J. Tailleur, and J. Huang, Cooperative pattern formation in multi-component bacterial systems through reciprocal motility regulation, *Nat. Phys.*, 1 (2020).
 - [12] M. H. Jacobs, *Diffusion Process* (Springer-Verlag, 1967).
 - [13] R. Zwanzig, Diffusion past an entropy barrier, *The Journal of Physical Chemistry* **96**, 3926 (1992).
 - [14] D. Reguera and J. M. Rubí, Kinetic equations for diffusion in the presence of entropic barriers, *Phys. Rev. E* **64**, 061106 (2001).
 - [15] D. Reguera, G. Schmid, P. S. Burada, J. M. Rubí, P. Reimann, and P. Hänggi, Entropic transport: Kinetics, scaling, and control mechanisms, *Phys. Rev. Lett.* **96**, 130603 (2006).
 - [16] P. S. Burada, G. Schmid, D. Reguera, J. M. Rubí, and P. Hänggi, Biased diffusion in confined media: Test of the fick-jacobs approximation and validity criteria, *Phys. Rev. E* **75**, 051111 (2007).
 - [17] X. Yang, C. Liu, Y. Li, F. Marchesoni, P. Hänggi, and H. P. Zhang, Hydrodynamic and entropic effects on colloidal diffusion in corrugated channels, *Proceedings of the National Academy of Sciences* **114**, 9564 (2017), <https://www.pnas.org/content/114/36/9564.full.pdf>.
 - [18] S. Marbach, D. S. Dean, and L. Bocquet, Transport and dispersion across wiggling nanopores, *Nature Physics* **14**, 1108 (2018).
 - [19] X. Yang, Q. Zhu, C. Liu, W. Wang, Y. Li, F. Marchesoni, P. Hänggi, and H. P. Zhang, Diffusion of colloidal rods in corrugated channels, *Phys. Rev. E* **99**, 020601(R) (2019).

- [20] P. S. Burada, G. Schmid, D. Reguera, M. H. Vainstein, J. M. Rubi, and P. Hänggi, Entropic stochastic resonance, *Phys. Rev. Lett.* **101**, 130602 (2008).
- [21] P. K. Ghosh, F. Marchesoni, S. E. Savel'ev, and F. Nori, Geometric stochastic resonance, *Phys. Rev. Lett.* **104**, 020601 (2010).
- [22] J. Elgeti and G. Gompper, Wall accumulation of self-propelled spheres, *EPL (Europhysics Letters)* **101**, 48003 (2013).
- [23] A. P. Solon, Y. Fily, A. Baskaran, M. E. Cates, Y. Kafri, M. Kardar, and J. Tailleur, Pressure is not a state function for generic active fluids, *Nature Physics* **11**, 673 (2015).
- [24] A. Duzgun and J. V. Selinger, Active brownian particles near straight or curved walls: Pressure and boundary layers, *Phys. Rev. E* **97**, 032606 (2018).
- [25] L. Caprini and U. Marini Bettolo Marconi, Active particles under confinement and effective force generation among surfaces, *Soft Matter* **14**, 9044 (2018).
- [26] L. Angelani, Confined run-and-tumble swimmers in one dimension, *Journal of Physics A: Mathematical and Theoretical* **50**, 325601 (2017).
- [27] C. G. Wagner, M. F. Hagan, and A. Baskaran, Steady states of active brownian particles interacting with boundaries (2021), [arXiv:2109.06353 \[cond-mat.soft\]](https://arxiv.org/abs/2109.06353).
- [28] N. Nikola, A. P. Solon, Y. Kafri, M. Kardar, J. Tailleur, and R. Voituriez, Active particles with soft and curved walls: Equation of state, ratchets, and instabilities, *Phys. Rev. Lett.* **117**, 098001 (2016).
- [29] H. Kramers, Brownian motion in a field of force and the diffusion model of chemical reactions, *Physica* **7**, 284 (1940).
- [30] A factor of $1/4$ appears because the particles can escape from two sides, and we only calculate the time ending at the peak of the entropy potential when particles have probability $1/2$ to escape.
- [31] J. Elgeti and G. Gompper, Self-propelled rods near surfaces, *EPL (Europhysics Letters)* **85**, 38002 (2009).
- [32] P. D. Neta, M. Tasinkevych, M. M. Telo da Gama, and C. S. Dias, Wetted of a solid surface by active matter, *Soft Matter* **17**, 2468 (2021).